A Direct Redundancy Approach to Fault-Tolerant Control of BLDC Motor With a Damaged Hall-Effect Sensor

Muhammad Aqil and Jin Hur, *Senior Member, IEEE*

***Abstract*—Often for a closed-loop operation of a brushless direct current (BLDC) motor, Hall-effect sensors are used and recently there have been a number of discussions on Fault-Tolerant Control (FTC) of the BLDC motor for a defective Hall-effect sensor. However, so far, direct redundancy based approach for FTC of BLDC motor for a position sensor fault is not presented. This paper contributes a direct redundancy based method by utilizing redundant Hall-effect sensors for FTC of a BLDC motor. Redundant Hall-effect sensors generate additional transitions resulting in faster fault detection. To verify the proposed idea, MATLAB/Simulink model is developed, and the simulation results are presented by programing a MATLAB function block acting as a fault-tolerant controller. Furthermore, the algorithm is implemented into the MicroLabBox for experimental validation, and the results are discussed.**

***Index Terms*—Brushless machines, fault-tolerant control (FTC), Hall-effect devices, position measurement, redundancy, signal reconstruction.**

I. Introduction

TRAPEZOIDAL voltage driven Brushless direct current (BLDC) motors are a type of permanent magnet synchronous motors (PMSM) that offer high efficiency, high-power volume ratios, low-maintenance costs, and use electronic commutation to energize the stator phases for generating electromagnetic torque. For the electronic commutation to work, the motor control circuit needs to know the rotor position at electrical 60° intervals to switch the stator phase currents [1], [2]. Each phase is active for two consecutive electrical 60° intervals, therefore, called as 120° commutation.

Often for commutation purposes, BLDC motors make the use of Hall-effect sensors to sense the rotor position [3]–[5]. During the normal operation of the motor system, the position sensor can become defective and may retain a constant value of one or zero, which will severely influence the motor operation causing either the motor to fail, drive to burn, or the system may come to a complete stop. In several applications, for example, electric vehicles, it is desirable to keep the system running even with degraded performance until the scheduled maintenance or help arrives [6]–[8]. A technique that keeps the motor system running, even after experiencing a sensor fault, is called a fault-tolerant control (FTC) system [9], [10]. Moreover, in aircrafts, it is difficult to reach to the motor for repairs, and in flight a sensor failure may create a dangerous situation; therefore, it would be preferable to have redundant sensors. The price of a single Hall-effect sensor is very low, and having redundant sensors will not cause a significant increase in the overall system cost. Thus, the method presented in this paper may be used for electric vehicles, electric scooters, and other myriad of applications of BLDC motors.

Hall-effect sensor fault effects on a BLDC motor drive are discussed, where value-based fault detection, Fast Fourier Transform (FFT), and spectral energy density (SED) are used for fault identification. Due to the use of FFT and SED, the recommended scheme takes 113 ms to diagnose and identify the fault [2]. Fast fault diagnosis technique is presented in [6], in which the Hall-effect sensor signals are sampled at high frequency and the sampling instants are treated as a rapid counter. Thus, whenever the counter limit is exceeded or falls behind the threshold values, there is a fault. The proposed technique offers fast fault diagnosis; however, there are acceleration limitations. Hall-effect sensor and signal injection technique is combined and suggests a fault robust speed estimation, which can be used in systems that comply with an Automotive Safety Integrity Level and Safety Integrity Level [11]. Nevertheless, the combined technique can only be used for motors with saliency and speeds greater than 0.1 p.u. In [12] and [13], an FTC method is presented; however, in some cases, the proposed technique can take up to 360 electrical degrees to identify the fault and moreover is computationally expensive because it uses the vector tracking observer and Fourier series for which computation of the Fourier coefficients is required. And furthermore in case of a multiple sensor fault, it is impossible to start the motor in the known direction; hence, the method cannot be used for applications in which there are frequent stops, such as electric scooters. Dong *et al*. [14] describe the Hall-effect sensor faults by presenting three different approaches. Approach one

Manuscript received November 16, 2018; revised January 30, 2019 and April 5, 2019; accepted May 3, 2019. Date of publication May 16, 2019; date of current version November 12, 2019. This work was supported in part by the Korea Institute of Energy Technology Evaluation and Planning and the Ministry of Trade, Industry & Energy of the Republic of Korea under Grant 20172010104790 and in part by the Industrial Strategic Technology Development Program of Korea Evaluation Institute of Industrial Technology under Grant 20002745. Recommended for publication by Associate Editor S. K. Panda. *(Corresponding author: Jin Hur.)*

The authors are with the Department of Electrical Engineering, Incheon National University, Incheon 22012, South Korea (e-mail: aqilafzal@hotmail.com; jinhur@inu.ac.kr).

Color versions of one or more of the figures in this paper are available online at http://ieeexplore.ieee.org.

Digital Object Identifier 10.1109/TPEL.2019.2917559

discusses the state-sensitive method where last three states of sensors are stored in memory and the controller keeps on comparing with the current state with the stored pattern and thus altered state sequence means that there is a fault; the second method proposes the use of sensor transition order by storing last two transitions in memory. A change in transition order points to a sensor fault. Method three works by following a condition-based approach which in some situations can also result in the diagnosis of wrong fault type until corrected after further operation of the motor. Although all three methods are simple but are based on the assumption that the motor is running continuously while the sensor fault occurs, which in certain applications may not be true. Also in some instances, the FTC method takes up to 10 ms till the corrective measures are taken and hence for 10 ms wrong commutation sequence is executed, generating large transient currents, which consequently result in large variations in speed. An FTC algorithm is designed, and simulation and experimental results are discussed. A set of virtual Hall-effect sensor signals is generated for each of the other two Hall sensors; furthermore, each pair of Hall sensor signals is checked for fault and compared with the other pair of Hall sensor signals. The sensor value, which remains constant as the rotor rotates, is diagnosed and identified as the faulty sensor. In the event of a fault, the virtually generated signal is replaced with the faulty sensors signal. The algorithm does not work for very low speeds and also recommends implementation as a standalone subsystem [15]. In [16], a Hall-effect sensor fault is detected by an acceleration threshold condition and identification of damaged sensor is performed using conditions, which are based on the fact that under healthy operation the sensor value must make transitions between high and low levels. However, it does not discuss the case when a fault happens and the threshold is not triggered or in the case that there is no transition and the sensor permanently maintains the value of 0 or 1. Furthermore, the methods that rely on the motor parameters such as sensorless algorithms are promising in terms of cost savings and reduction of components count, however, suffering from parameter variations. Complex algorithm and computations of the sensorless algorithms require high-end digital signal processors (DSP). The sensorless technique works well for the motors that have saliency, whereas for non-salient motors sensorless control gives poor results at low speeds or with load variations [17].

II. FTC by Direct Redundant Hall-Effect Sensors

As per the author's knowledge, direct redundancy [18] approach to FTC of BLDC motor is not applied to date. In this paper, a Hall-effect sensor FTC approach is presented, which exploits the idea of direct redundancy by using six Hall-effect sensors, as shown in Fig. 1. Six Hall-effect sensors are divided into two groups, group one of primary sensors and group two of secondary sensors. Primary Hall- effect sensors P1, P2, and P3 are employed to commutate the stator phase currents, whereas the secondary sensors S1, S2, and S3 serve for fast fault detection and speed estimation after the failure of the one of the primary sensor. The direct redundant method offers the benefits as follows.

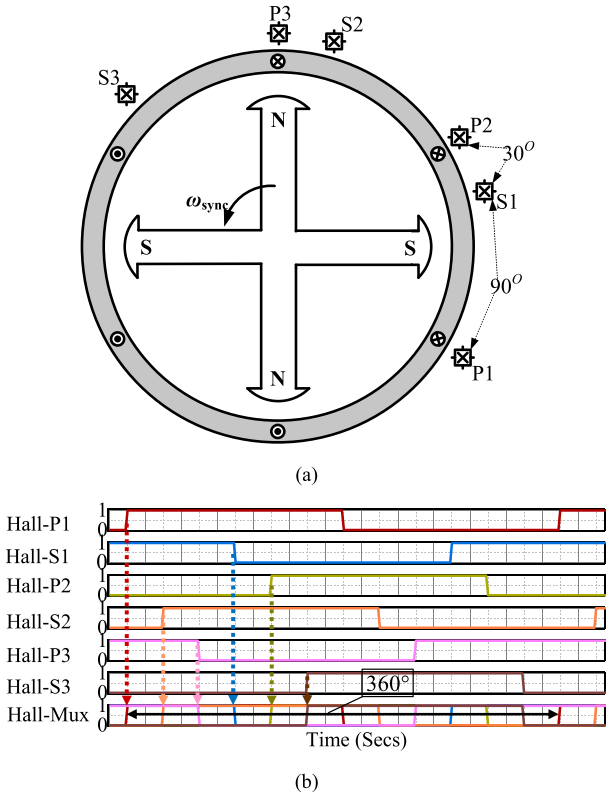

Fig. 1. Illustration of the concept showing sensor placement and resultant signals. (a) Diagram of the proposed idea. (b) Signals of the direct redundant Hall-effect sensors. Stacked individual sensor signals are multiplexed showing 12 transitions in one electrical revolution.

1) A transition at every electrical 30° offers faster fault diagnosis and identification (FDI), thus reducing total compensation time.
2) Computationally less expensive compared to the methods that use Fourier series or Park/Clark transformation and hence not requiring high-end processors for complex computations.
3) Robust because it only depends on Hall-effect sensor signals and not on motor parameters.

After experiencing a single sensor fault in a motor with three Hall-effect sensors, the system's position accuracy is decreased from 60 to 90 electrical degrees; consequently, it is very difficult to determine the rotor position using the two Hall-effect sensors. Thus, at any time under fault conditions either it is risky or impossible to start the motor in a known direction, once the motor comes to a complete stop.

Contrary to the three sensors, direct redundant sensors idea solves this issue of starting the motor in the known direction, elegantly. If one of the primary sensors becomes defective, nevertheless leaving five healthy sensors providing the necessary rotor position information, to start the motor in the known direction.

III. Hall-Effect Sensor Faults

Hall-effect sensor can become defective at any instant throughout the operational life of the BLDC motor. Considering

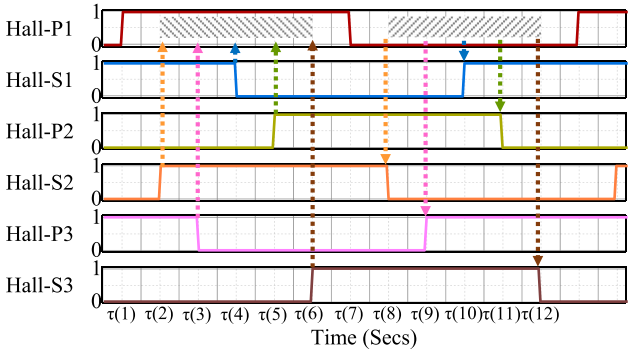

Fig. 2. Value of P1 with respect to the transitions of all the sensors including P1.

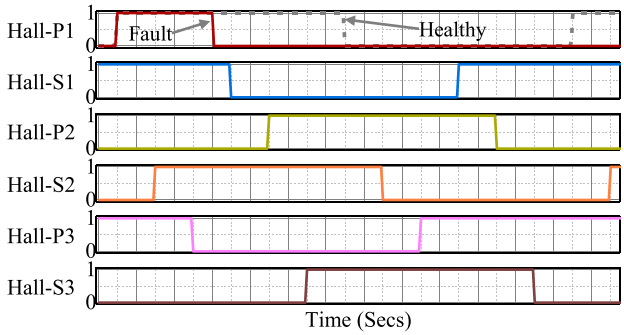

Fig. 3. Faulty transition lies in the prohibitive area; hence, there will be no irregular motor phase currents as the controller time constant is very small compared to the motor's mechanical time constant.

the Hall-effect sensor fault, it is assumed that either the sensor value remains one or zero, for the rest of the operation of the system. Therefore, a single sensor fault can be divided into essentially four cases. First, sensor retaining the value of zero after the incorrect transition; second, sensor remains one permanently and no longer switches between the states; third, the sensor changes its value from zero to one earlier than the supposed transition time and becoming constantly one; and finally, the sensor's output falls from one to zero before its assumed time of transition and remaining zero till the system operation lasts.

Hall-effect sensor assembly of BLDC motors (see Fig. 1) illustrates that when the rotor rotates, Hall-effect sensor values change with respect to the fixed mechanical location of the rotor; therefore, the mechanical assembly of the sensors and motor can be called as a rigid system. The important point here is that the values of the rest of the sensors at a particular transition are static and are mechanically constrained. For example, as shown in Fig. 1(b), the primary sensor P1 has high value for the transitions S2F, P3F, S1R, P2R, and S3F (here, sensor edge naming convention is followed such that first alphabet is sensor group i.e., primary or secondary, numeral is a sensor number, e.g., 1, 2, or 3, and the last alphabet is the edge type either falling or rising edge) as long as the direction of rotation does not change and system is working normally. Therefore, at the transitions S2F, P3F, S1R, P2R, S3F, the primary sensor P1 is detected as low, and at transitions S2R, P3R, S1F, P2F, S3R, the primary sensor P1 has high value, which spontaneously points to a faulty P1 sensor. Thus for a particular sensor, there is only and only one combination (or set) of sensor transitions possible during its low value, whereas for the high value it is complementary of low value, as is shown in Fig. 2. Therefore, for each sensor, two areas can be defined where a transition is impermissible under normal operation and are named as prohibitive areas; the first area is for the low value of the sensor, and the second area is for the high value of the sensor. From Fig. 2, it can be observed that for the specific case of the primary sensor P1, which has fixed value at particular transitions, i.e., for transitions at time $\tau(2)$, $\tau(3)$, $\tau(4)$, $\tau(5)$, and $\tau(6)$, the primary sensor P1 will have explicitly high value and similarly for the low value of P1.

As explained earlier that the motor and Hall-effect sensor assembly is a rigid system, therefore, in a healthy state of the system for an individual sensor, any transition in the constrained area is prohibited and is not possible. Nevertheless, a damaged sensor can have a falling or rising edge inside the constrained area, as shown in Fig. 3. A false transition outside mechanically constrained area has two possibilities. First, the sensor output rises before the real transition time as in Fig. 4(a); second, it has the correct rising edge; however, it becomes defective and falls in advance of the mechanically constrained area, as shown in Fig. 4(b). Case one is further divided into inhibitive transition time and acceptable transition time as shown in Fig. 4(c) and (a), respectively. Although the transition in Fig. 4(b) belongs to a damaged sensor, nevertheless, it is accepted on the basis that it is within the buffer time. It was observed in experimentation that the Hall-effect sensor transitions are not equidistance even at constant speed operation; therefore, the concept of buffer time is adapted to avoid unnecessary complications, which can be an area of further research. A false transition of a defective sensor is acceptable when it is within 15 electrical degrees of the supposed sensor transition time. In other words, the change in speed caused by the incorrect transition is less than or equal to 1.5 times the last correct speed reading. And finally, Fig. 5(a) illustrates the possibility that the sensor retaining zero value permanently and 5(b) shows the sensor value staying at a high level.

IV. Fault Detection and Identification

As depicted in Fig. 6(a), there is twice the number of transitions in comparison to the three Hall-effect sensor-based methods [see Fig. 6(b)], and as a consequence providing more transition instants to check for damaged sensors in the redundant Hall-effect sensor-based approach, thus faster detection of the fault. In Fig. 7, the flowchart of the proposed fault detection, identification, and compensation process is shown. Fault detection is classified into two methods, one is the speed-dependent method and the second method relies upon by calling the motor and Hall-effect sensor assembly as a mechanically rigid system and thus having a transition prohibitive area. When the system operates normally, a sensor develops a defect, the FDI process detects and identifies the fault, sector width is adjusted in the zeroth-order speed estimation algorithm, and finally, based on the estimated speed, the missing sensors transition instants are

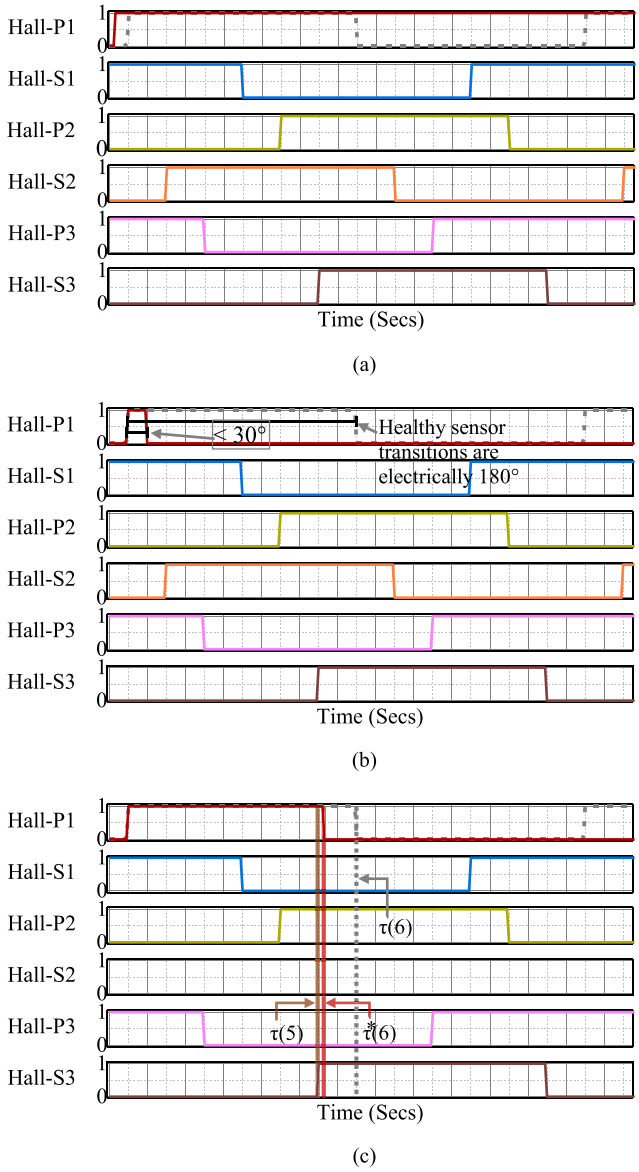

Fig. 4. Incorrect commutation of the motor phase current w.r.t. to the location of the transition: (a) Transition is outside the mechanically constrained area and causes the maximum motor transient currents. (b) Transition is outside the prohibited area, resulting in no erroneous motor phase currents. (c) Faulty transition is detected by the FTC system, hence causing no irregular commutation.

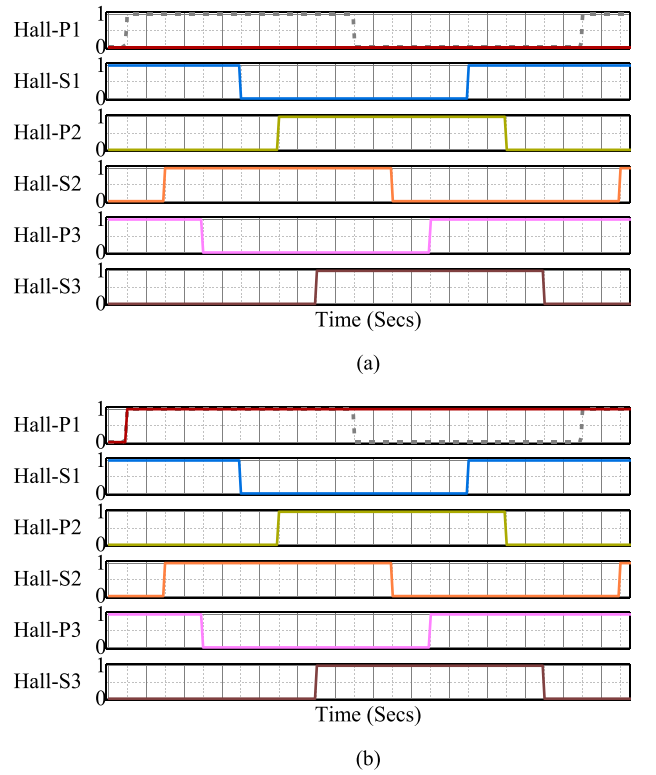

Fig. 5. P1 = 0 and P1 = 1 fault. (a) Hall-effect sensor experiences a fault and after that remains zero. (b) The case that the sensor retains the value one after experiencing the fault.

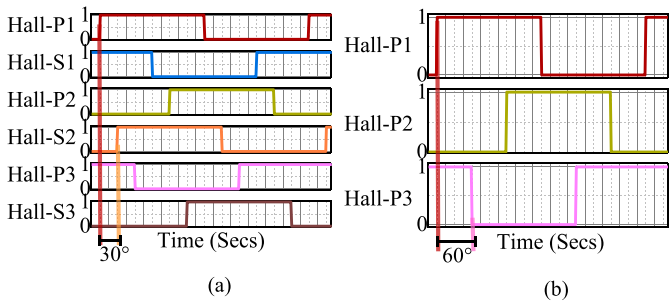

Fig. 6. Comparison of the direct redundant Hall sensor method with the Three-Hall sensor method. (a) Six Hall-effect sensors provide a transition every 30 electrical degrees. (b) Three Hall-effect sensors result in 60 electrical degree transitions.

predicted and virtually regenerated by the controller, which are explained in detail in the next sections.

A. *Speed-Based Fault Detection*

In drive systems with Hall-effect sensors, the rotor position is exclusively determined at the transition instances and each set of consecutive transitions of the Hall-effect sensors correspond to a fixed distance on the rotor, and therefore, only at transition instants, rotor speed is updated. Mechanical speed of a synchronous motor is given by

$$n_m = \frac{120 * f_e}{P} \tag{1}$$

where f_e is the electrical frequency, in Hz, n_m is the mechanical rotor synchronous speed, r/min, and P is the number of rotor poles [19].

For redundant Hall-effect sensor application, there are 12 transitions in one electrical period, therefore, (1) becomes

$$n_m = \frac{120}{12 * T_e * P} \tag{2}$$

where $T_e = 1/f_e$ and T_e is the time interval between the two consecutive transitions. Whenever there is a change in the time period between two consecutive transitions, it results in modified speed reading. Conversely, speed change will result in change in time between the two consecutive transitions, i.e., T_e.

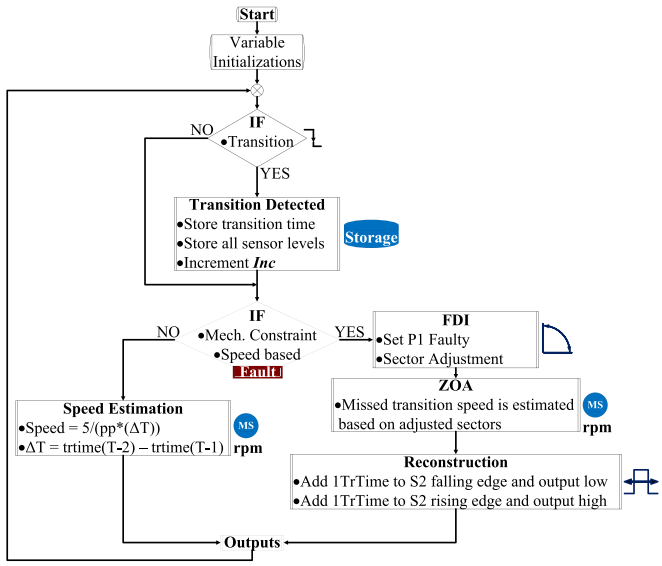

Fig. 7. Flowchart of the proposed FTC method.

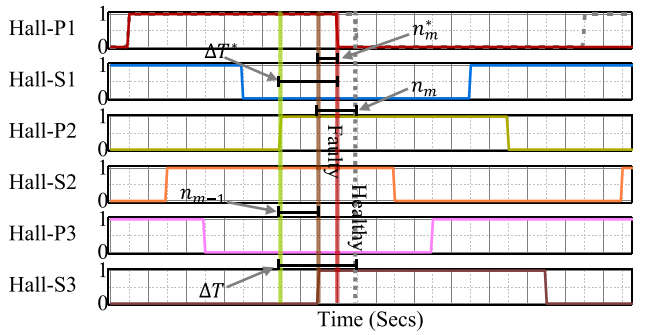

Fig. 8. Incorrect edge causes a change in the transition times. As a result, the altered speed is mentioned as well.

A sensor that failed to function properly, transitions outside the mechanically constrained area, is detected and identified, based on the distance from the previous correct transition. Since every two transitions are 30 electrical degrees apart, therefore, the time between the two consecutive transitions is dependent on the speed of the motor. Thus, an incorrect transition that is too close to the last healthy transition will provide a very high-speed estimate giving a large acceleration reading, as shown in Fig. 4(c). Motor acceleration is given by

$$a_{cc} = \frac{n_{m-1} - n_m}{\Delta T} \tag{3}$$

where n_{m-1} is the speed estimate based on the last two consecutive transitions, n_m is the speed estimate based on the preceding and current transition, and ΔT is the time between the two speed readings, as depicted in Fig. 8. Acceleration under normal constant speed operation is zero. And when there is a fault, (3) becomes

$$a_{cc} = \frac{n_{m-1} - n_m^*}{\Delta T^*} \tag{4}$$

where n_m^* is the modified speed reading based on incorrect and last healthy transition and ΔT^* is the time between the last and faulty speed reading.

As shown in Fig. 4(c), there is a very small time difference between the Hall-effect sensor S3's rising edge and the defective Hall-effect sensor P1's falling edge, which will provide the motor controller with very high speed and acceleration reading. Here an assumption can be made that the maximum possible acceleration the motor can attain is during the no-load startup. Therefore, the condition to detect defective transition is founded on the no-load startup acceleration, i.e., when the incorrect transition of the damaged sensor causes the motor controller to have the reading, which exceeds the no-load startup acceleration, thereby indicating a defective sensor, and the condition is shown in the following equation:

$$a_{cc} \leq a_{st} \tag{5}$$

where a_{cc} is the current acceleration reading, and a_{st} is the motor start-up acceleration. As the speed estimation is done by assuming that each pair of consecutive transitions corresponds to a fixed mechanical rotor distance, a faulty transition results in very high speed and acceleration reading since the controller assumes that the two transitions correspond to 30 electrical degrees; however, the time difference between the false transition and last normal transition is very small. In speed-based fault detection and identification, no false motor phase currents are observed, i.e., when constant speed operation of the system is considered.

Fig. 4(b) depicts the event that incorrect transition occurs merely before the mechanical constrained area. The mechanical rotor distance between the rising and falling edge, of any of particular sensor, corresponds to 180 electrical degrees; however, in the case of Fig. 4(b), the distance between the healthy and inaccurate transition, is less than 30 electrical degrees, which results in the controller getting improper acceleration reading relative to the last acceleration value. Thus, this fault is detected based on the incorrect acceleration reading and hence the detection results in no imprecise motor phase currents.

Fig. 5(a) illustrates the event of a faulty transition not detected by the startup acceleration limit; however, is a faulty transition and will trigger incorrect motor phase currents of less than 15 electrical degrees before the mechanically constrained area and spurious motor phase currents of 30 electrical degrees after the mechanically constrained area; this fault causes the maximum electrical degrees for which the motor conducts faulty phase currents. And the fault is detected at the falling edge of sensor S2.

B. Fault Detection by Mechanical Constraint

The idea of mechanical constraint was explained previously, thus it is not explained here to avoid restatement. In the outcome that a wrong transition of a damaged sensor occurs inside the mechanically prohibitive area, this incorrect transition is detected momentarily and produces no false conduction of motor phase currents, owing to the fact that controller time constant is much smaller than the motor time constant. And thus, the motor operation is not affected.

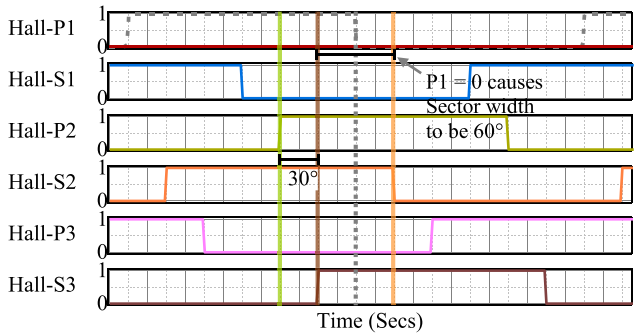

Fig. 9. P1 = 0 fault w.r.t. to the six Hall-effect sensors, showing change in sector width after the occurrence of the fault.

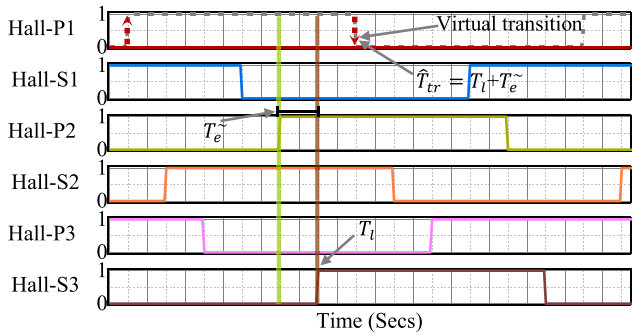

Fig. 10. Estimation of transition instant in case of a sensor fault in zeroth-order algorithm and respective variable definitions.

Finally, the sensor value remaining zero, uninterruptedly, will be detected at the start of the following mechanically constrained area, resulting in 30 electrical degrees of the faulty conduction of the motor phase currents. The case of sensor value constantly one is similar to the sensor value continually zero, and it will similarly cause incorrect phase currents of 30 electrical degrees.

V. Fault Tolerance With Zeroth-Order Algorithm

Hall-effect sensors provide information about rotor location at discrete instances, thus requiring a technique to reconstruct the speed signal of the motor. For this reason, data hold method is employed. In order to reconstruct a signal, its power series expansion is performed. Higher order terms in the power series expansion of the signal provide good reconstruction of the signal; however, requiring more resources and leading to more delays in the control loop. Introduction of the delays in the control loop can cause severe system stability problems. Therefore, the first term of the power series is often used for reconstruction of signal and hence the name zeroth-order hold. Information on the signal is only available at the sample instants, i.e., speed signal is updated on each Hall-effect sensor transition [20].

After the fault is diagnosed and the sensor is identified, it is desirable to regenerate the missing sensors signal in order to keep the motor operating. The defective sensor does not generate transitions any longer, therefore requiring the redefinition of the sector width in the zeroth-order algorithm to have correct speed estimation and consequently the regeneration of the missing sensor's signal. Sector width redefinition is shown in Fig. 9. Under a single sensor fault condition, for the case of the redefined sector width, the speed is estimated as

$$n_m = \frac{2 * 120}{12 * T_e * P}. \tag{6}$$

For regeneration of the missing edge, prior speed estimate of the P2 and S3's transitions is used to predict the estimated time of the missed transition and the time is calculated by

$$T_e^{\sim} = \frac{120}{12 * n_m * P} \tag{7}$$

where $T_e^{\sim}$ is the estimated time between two consecutive transitions.

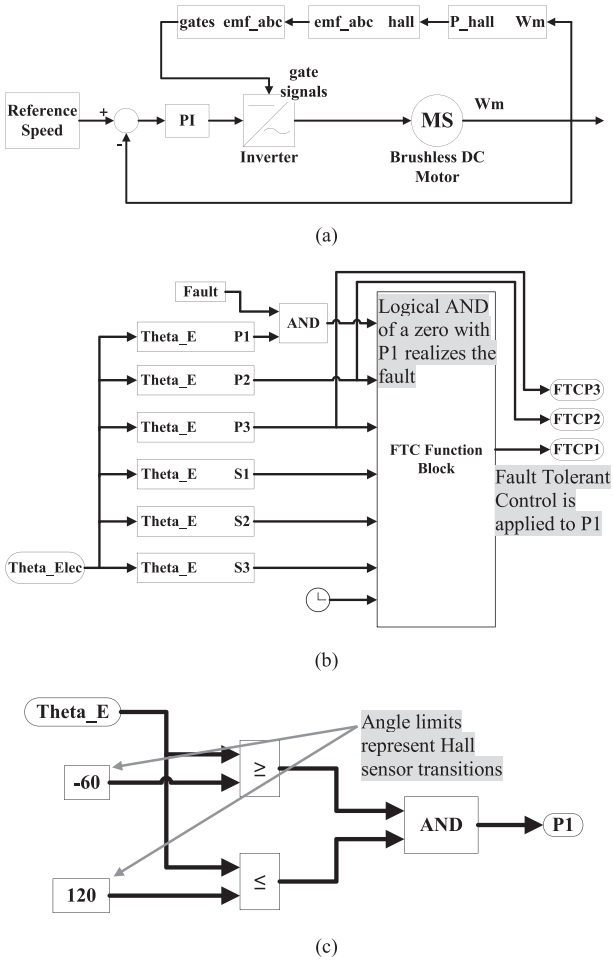

Fig. 11. MATLAB/Simulink simulation: (a) Block diagram of the complete simulation. (b) Implementation of FTC and fault. (c) Realization of Hall-effect sensors by using limits and relational operators.

To generate the edge, one transition time $T_e^{\sim}$ is added to the last transition time and when the current time (for time keeping, internal clock of controller is used) is equal to the last transition time plus one transition time, it determines the estimated transition instant, as shown in Fig. 10. In terms of an equation, we

TABLE I
SIX-POLE BLDC MOTOR PARAMETERS

Parameter Name	Value
Stator phase resistance, R_a	0.07 ohm
Stator phase inductance, L_a	0.9386 mH
Rated torque	1.1 N·m
Rated current	10.32 Amps
Rated voltage	48 V
Rotor inertia	2.28×10^{-4} N·m·s^2

obtain

$$\hat{T}_{\rm tr} = T_l + T_e^{\sim} \tag{8}$$

where T_l is the time of last transition instant, and $\hat{T}_{\rm tr}$ is the estimated time of transition instant.

VI. SIMULATION RESULTS AND DISCUSSION

MATLAB/Simulink simulation is performed to validate the purposed idea. A MATLAB built-in simulation of a BLDC motor is used, and a MATLAB function block is added to the simulation and is programmed to simulate the FTC, as shown in Fig. 11(a). Table I mentions a six-pole BLDC motor that is used in the simulation and the motor parameters are given.

A PI controller controls the motor speed by generating the control signal after comparing the current motor speed with the reference speed and thus supplies the motor with the necessary input voltage. To construct the six Hall-effect sensor signals, mechanical speed is converted to electrical speed by

$$f_e = \frac{120 * n_m}{P} \tag{9}$$

where P is the number of poles of the rotor. Integration of the electrical frequency f_e converts it into the rotor electrical position. This electrical position is then compared with constant limits to generate the six discrete Hall-effect sensor signals, and the fault is realized by Logical-AND or Logical-OR of sensor output with logical one or logical zero, generated by comparing fault time with the current simulation time, as shown in Fig. 11(b) and (c), respectively. Subsequently, these six signals are fed to the FTC block, which handles the sensor faults and compensates for the damaged sensor by generating a virtual signal, as depicted in the flowchart of the FTC process.

In terms of the FTC system response to a fault, the method is divided into three categories. First, the faults whose response is so swift that it results in no transients in motor phase currents and the motor speed; second, faults that cause incorrect motor phase currents of 30 electrical degrees; and finally, the faulty motor phase currents last for approximately 45 electrical degrees.

Fig. 12 shows the response of the simulation in case of a single sensor fault. The reference speed for BLDC motor is set at 2000 r/min with 0.3 N·m load. A P1 = 0 fault initiates at $t = 0.2485$ s. The fault causes false motor phase currents, which results in a speed transient of approximately 25 r/min at 0.255 s and lasts for 30 ms approximately. The fault time

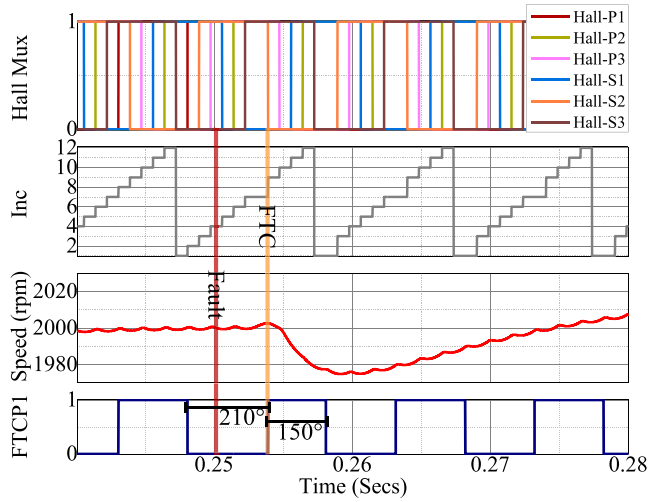

(a)

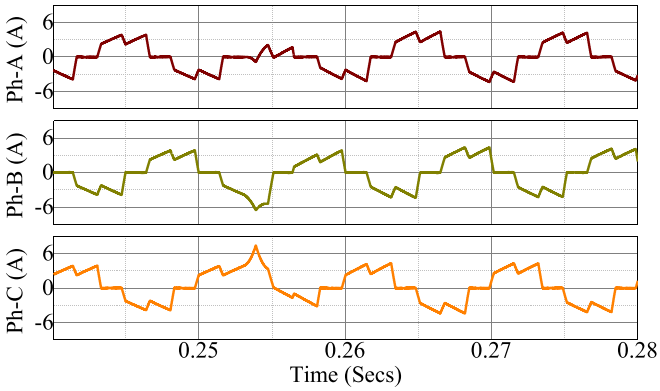

(b)

Fig. 12. P1 = 0 fault causes 30 electrical degrees of false motor phase currents. (a) FTC systems response. (b) Motor phase currents in response to the fault.

was set at 0.2485 s; however, the transient starts at 0.255 s, and the reason for that is that there is no transition until 0.2539 s and therefore the fault is detected at the start of the mechanical constrained area, which results in 30 electrical degrees of false motor phase currents. The constrained area starts at the transition of sensor S2 and the FTC process takes 0.83 ms. The fault that the sensor constantly remains one will result in similar transients as described for the case of sensor consistently remaining zero.

In the event that a sensor has a transition as well as stops functioning properly and is not detected by the speed condition or by the mechanical constraint will cause maximum transient currents in motor phases of equal to or less than approximately 45 electrical degrees. The Hall-effect sensor signal will be similar to as depicted in Fig. 4(a). Fig. 13 shows the response of the FTC algorithm and the motor phase currents. The single sensor fault initiates at time $t = 0.2477$ s and results in speed transient of 20 r/min and lasts for 60 ms approximately. Finally, when the improper transition of a malfunctioning sensor has a transition in a prohibited area at $t = 0.246$ s will be detected, identified, and compensated so quickly that it causes no speed or phase

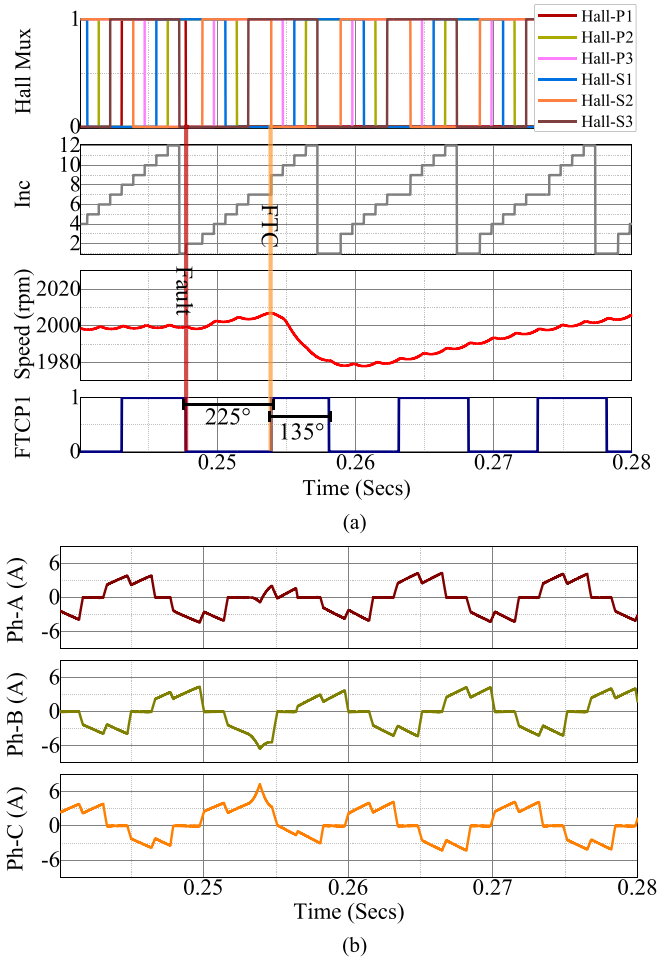

Fig. 13. Fault that goes undetected by the speed condition or mechanical constraint causes the maximum electrical degrees of conduction of incorrect motor phase currents. (a) FTC algorithms response. (b) Transients in motor phase currents.

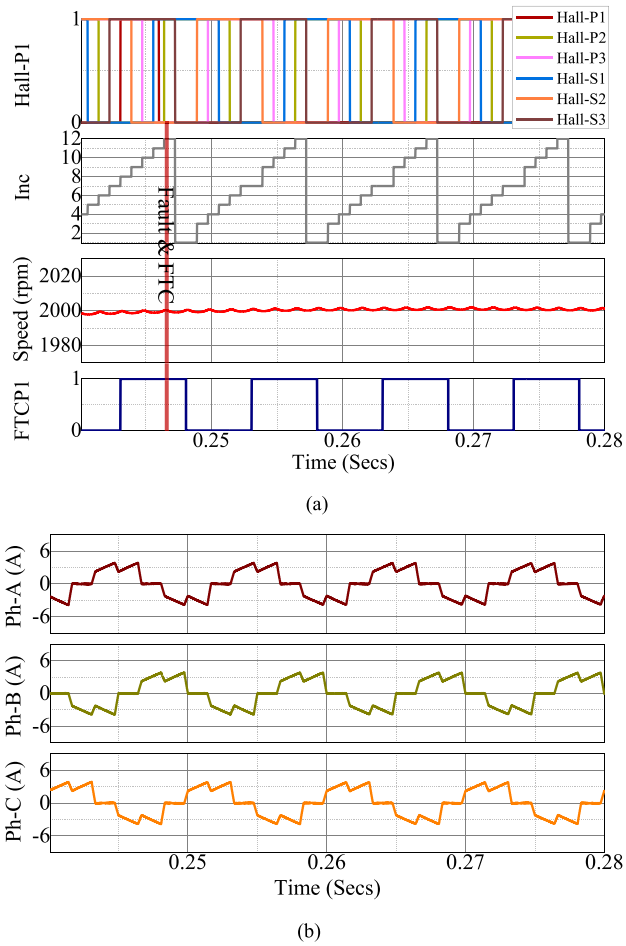

Fig. 14. Incorrect transition in the prohibitive area; the motor operation is not affected. (a) FTC response of the algorithm. (b) Motor phase currents.

current transients and is shown in Fig. 14. The motor maintains its normal operation before and after the occurrence of the fault.

VII. Experimental Verification of the Algorithm

For experimental validation of the algorithm, six Hall-effect sensors are soldered on two PCBs. The PCBs are rotated by 30 mechanical degrees with reference to the primary Hall-effect sensors PCB, thus providing a 90 electrical degree Hall-effect sensor signals for a 6-pole BLDC motor, as shown in Fig. 15. Fig. 16 pictures the FTC model that was built and downloaded into the MicroLabBox DS-1202. Fig. 17 shows a 6-pole BLDC motor coupled to a dc motor to generate the Hall-effect sensor signals. Hall-effect sensors are connected to the fixed 5 V and the dc motor is powered by the variable output dc power supply. The six sensor signals are then fed to six analog-to-digital channels of MicroLabBox DS-1202. Sensor fault is realized by passing P1 sensor's signal from an ON–OFF switch. Class 1 analog-to-digital channels from 1 to 6 are used to receive the Hall-effect sensor signals. Since the received signals by the MicroLabBox DS-1202 are scaled, Hall-effect sensor signals

Fig. 15. Six Hall-effect sensors mounted at two PCBs at 30 mechanical degrees apart; the magnetic disc is removed.

are passed through the gain blocks, in order to have appropriate amplitudes and are then fed to the FTC function block, which handles the sensor faults [21]. The FTC method is implemented for P1 sensor only in anticipation that for the rest of the sensors it will be similar.

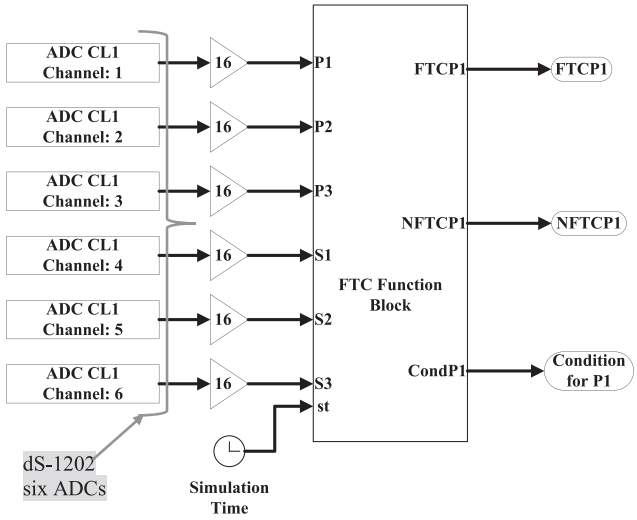

Fig. 16. Six channels of the MicroLabBox DS-1202 are connected to the six sensor outputs.

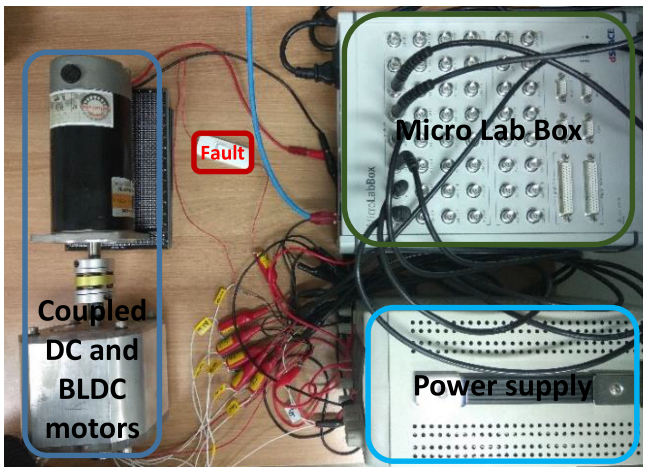

Fig. 17. Experimental setup of the system. BLDC motor is coupled with the dc motor and the sensor outputs are connected with the MicroLabBox DS-1202's six channels. And the fault is realized by an ON–OFF switch.

Experimental results obtained from the MicroLabBox DS-1202 are monitored in the dSPACE ControlDesk-5.5 and are shown in Fig. 18. At approximately 0.345 s, the fault switch is turned OFF, thereby mimicking a malfunctioning sensor. In the close-up view in Fig. 18(b), it can be seen that the incorrect transition occurs at 0.345 s, nevertheless the condition for P1 variable raises up after a delay of approximately 300 μs and that is for the reason that the damaged sensor is detected at the oncoming falling edge of sensor P3. The time when the fault is diagnosed and identified, i.e., as soon as the condition for P1 rises, at the same moment the FTC algorithm initiates the damaged sensor's virtual signal and the overall process takes approximately 400 μs. This experiment was performed at approximately 200 r/min. The limit for the minimum value of the sample time for Controldesk5.5NG and MicroLabBox DS-1202 is 0.1 ms; as a result, the experimentation was done at a low speed [22].

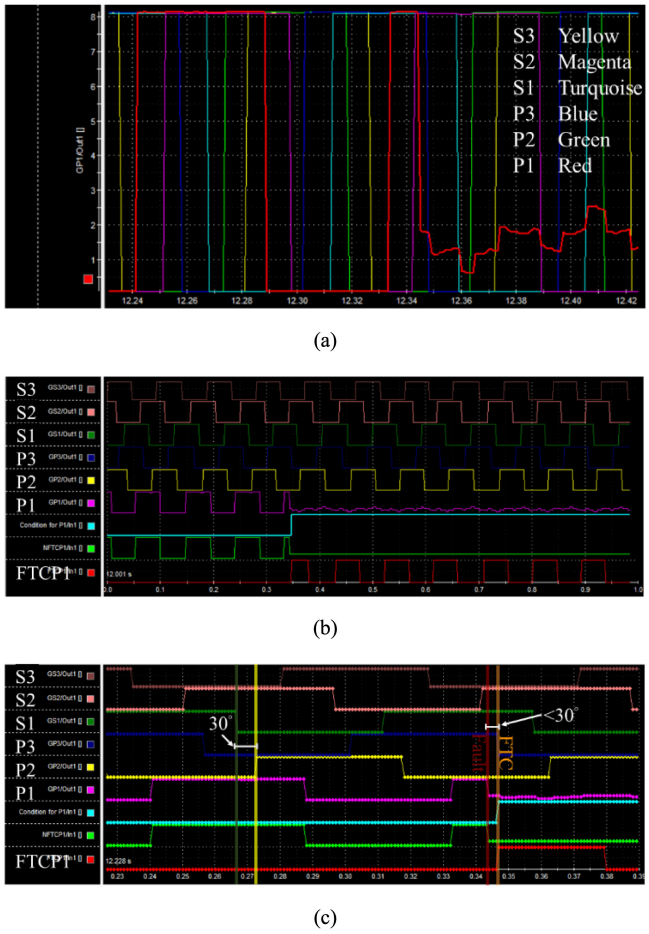

Fig. 18. Screenshots of the Controldesk-5.5 showing Hall-effect sensor fault and the FTC process: (a) Hall-effect sensor transitions are multiplexed. (b) The stacked view of the sensor signals, the fault condition, and the compensated signal generated by the FTC. (c) Stacked signals in close-up view.

VIII. Conclusion

Transitions of the redundant Hall-effect sensors provide supplementary opportunities to detect faults within electrical 30° or in the worst case in electrical 45° and therefore the proposed FTC method results in faster fault compensation times as the experimental results show that the compensation is done in less than electrical 30°. Compared to other FTC methods that use Fourier coefficients and FFT calculations, requiring high-end DSPs, this method offers less complexity, improved compensation time, and reduces the computational costs; however, the use of direct redundancy does increase the system cost slightly.

And furthermore, in recent research, for the constant speed operation of BLDC motor, the Hall-effect sensor transitions are assumed to be equally spaced; however, experiments showed that transitions are not equally spaced, which makes implementation of the FTC process more complicated. To name a few reasons, there can be misaligned Hall-effect sensors or cogging torque. Since the redundant sensor method presented here only considers the Hall-effect sensor signals, in that matter, the method presented in this paper offers robustness and simplicity.

REFERENCES

[1] J. Chiasson, *Modeling and High-Performance Control of Electric Machines*, Hoboken, NJ, USA: Wiley, 2005.

[2] A. Tashakori and M. Ektesabi, "A simple fault tolerant control system for Hall effect sensors failure of BLDC motor," in *Proc. IEEE Conf. Ind. Electron. Appl.*, Melbourne, VIC, Australia, 2013, pp. 1011–1016.

[3] Q. Zhang and M. Feng, "Combined commutation optimisation strategy for brushless DC motors with misaligned Hall sensors," *IET Elect. Power Appl.*, vol. 12, no. 3, 2017, pp. 301–307.

[4] X. Song, J. Fang and B. Han, "High-precision rotor position detection for high-speed surface PMSM drive based on linear Hall-effect sensors," *IEEE Trans. Power Electron.*, vol. 31, no. 7, pp. 4720–4731, Jul. 2016.

[5] S.-Y. Kim, C. Choi, K. Lee, and W. Lee, "An improved rotor position estimation with vector-tracking observer in PMSM drives with low-resolution Hall-effect sensors," *IEEE Trans. Ind. Electron.*, vol. 58, no. 9, pp. 4078–4086, Sep. 2011.

[6] Q. Zhang and M. Feng, "Fast fault diagnosis method for Hall sensors in brushless dc motor drives," *IEEE Trans. Power Electron.*, 2018, vol. 34, no. 3, pp. 2585–2596, Mar. 2019.

[7] J. G. Cintron-Rivera, S. N. Foster, and E. G. Strangas, "Mitigation of turn-to-turn faults in fault tolerant permanent magnet synchronous motors," *IEEE Trans. Energy Convers.*, vol. 30, no. 2, pp. 465–475, Jun. 2015.

[8] H. Li, W. Li, and H. Ren, "Fault-tolerant inverter for high-speed low-inductance BLDC drives in aerospace applications," *IEEE Trans. Power Electron.*, vol. 32, no. 3, pp. 2452–2463, Mar. 2017.

[9] H. Alwi, C. Edwards, and C. Pin Tan, "Chapter 2—Fault tolerant control and fault detection and isolation," in *Fault Detection and Fault-Tolerant Control Using Sliding Modes*. Berlin, Germany: Springer, 2011.

[10] M. Blanke, M. Staroswiecki, and N. E. Wu, "Concepts and methods in fault-tolerant control," in *Proc. Amer. Control Conf.*, Arlington, VA, USA, Jun. 2001, pp. 2606–2620.

[11] G. D. Donato, G. Scelba, M. Pulvirenti, G. Scarcella, and F. G. Capponi, "Low-cost, high-resolution, fault-robust position and speed estimation for PMSM drives operating in safety-critical systems," *IEEE Trans. Power Electron.*, vol. 34, no. 1, pp. 550–564, Jan. 2019.

[12] G. Scelba, G. De Donato, M. Pulvirenti, F. G. Capponi, and G. Scarcella, "Hall-effect sensor fault detection, identification, and compensation in brushless dc drives," *IEEE Trans. Ind. Appl.*, vol. 52, no. 2, pp. 1542–1554, Mar./Apr. 2016.

[13] G. Scelba, G. De Donato, G. Scarcella, F. G. Capponi, and F. Bonaccorso, "Fault-tolerant rotor position and velocity estimation using binary Hall-effect sensors for low-cost vector control drives," *IEEE Trans. Ind. Appl.*, vol. 50, no. 5, pp. 3403–3413, Sep./Oct. 2014.

[14] L. Dong, J. Jatskevich, Y. Huang, M. Chapariha, and J. Liu, "Fault diagnosis and signal reconstruction of Hall sensors in brushless permanent magnet motor drives," *IEEE Trans. Energy Convers.*, vol. 31, no. 1, pp. 118–131, Mar. 2016.

[15] V. Sova, J. Chalupa, and R. Grepl, "Fault tolerant BLDC motor control for Hall sensors failure," in *Proc. 21st Int. Conf. Autom. Comput.*, Glasgow, U.K., 2015, pp. 1–6.

[16] L. Dong, Y. Huang, J. Jatskevich, and J. Liu, "Improved fault-tolerant control for brushless permanent magnet motor drives with defective Hall sensors," *IEEE Trans. Energy Convers.*, vol. 31, no. 2, pp. 789–799, Jun. 2016.

[17] S. Noguchi, H. Mabuchi, K. Suzuki, and H. Dohmaeki, "Study of parameter variations compensation in sensorless control of PMSM," in *Proc. 19th Int. Conf. Elect. Mach. Syst.*, Chiba, Japan, 2016, pp. 1–6.

[18] J. W. Bennett, B. C. Mecrow, A. G. Jack, and D. J. Atkinson, "A prototype electrical actuator for aircraft flaps," *IEEE Trans. Ind. Appl.*, vol. 46, no. 3, pp. 915–921, May/Jun. 2010.

[19] S. J. Chapman, *Electric Machinery Fundamentals*. New York, NY, USA: McGraw-Hill, 2005.

[20] K. Ogata, *Discrete-Time Control Systems*, Englewood Cliffs NJ, USA: Prentice-Hall, 1995.

[21] C. Grigas, "Troubleshooting common tech support issues - dSPACE," dSPACE, Mar. 6, 2015. [Online]. Available: https://www.dspace.com/en/inc/home/news/blog-inc_1503.cfm. Accessed: Oct. 26, 2018.

[22] K. A. Lilienkamp, *Lab Experiences for Teaching Undergraduate Dynamics*. Cambridge, MA, USA: MIT Press, 2003.

Muhammad Aqil received the M.Sc. degree in electrical engineering from Northern Illinois University, DeKalb, IL, USA, in 2012. Since 2017, he has been working toward the Ph.D. degree in electrical engineering with Incheon National University, Incheon, South Korea.

During the M.Sc. degree, he was a Research Assistant with Northern Illinois University for the Argonne National Lab's upgrade project to improve the analog control system of the electromagnets to high-resolution digital control systems. From 2012 to 2015, he was a Manufacturing Engineer with a plant in Chicago, IL, USA. From 2015 to 2017, he taught the courses of electromagnetic theory, thermodynamics, and C programming language with International Islamic University Islamabad and Riphah International University, Islamabad, Pakistan. His current research interest is motor faults and fault-tolerant control for motor drive systems.

Jin Hur (SM'03) received the Ph.D. degree in electrical engineering from Hanyang University, Seoul, South Korea, in 1999.

From 1999 to 2000, he was with the Department of Electric Engineering, Texas A&M University, College Station, TX, USA, as a Postdoctoral Research Associate. From 2000 to 2001, he was a Research Professor of electrical engineering for BK21 projects with Hanyang University. From 2002 to 2007, he was the Director of Intelligent Mechatronics Research Center, Korea Electronics Technology Institute, Puchon, South Korea, where he worked on the development of special electric machines and systems. From 2008 to 2015, he was an Associate Professor with the School of Electric Engineering, University of Ulsan, Ulsan, South Korea. Since August 2015, he has been a Professor with the Department of Electrical Engineering, Incheon National University, Incheon, South Korea. He is the author of more than 140 publications on electric machine design, analysis and control, and power electronics. He has one granted pending US patent and 20 granted pending Korean patents. His current research interests include high-performance electrical machines, modeling, drives, new concept actuators for special purposes, and numerical analysis of electromagnetic fields.

Dr. Hur is currently an Associate Editor for the IEEE TRANSACTION ON POWER ELECTRONICS.